

DIVERSITY OF LUMINOUS SUPERNOVAE FROM NON-STEADY MASS LOSS

TAKASHI J. MORIYA^{1,2,3} AND NOZOMU TOMINAGA^{4,1}*Draft version November 10, 2018*

ABSTRACT

We show that the diversity in the density slope of the dense wind due to non-steady mass loss can be one way to explain the spectral diversity of Type II luminous supernovae (LSNe). The interaction of SN ejecta and wind surrounding it is considered to be a power source to illuminate LSNe, because many LSNe show the wind signature in their spectra (Type IIn LSNe). However, there also exist LSNe without the spectral features caused by the wind (Type IIL LSNe). We show that, even if LSNe are illuminated by the interaction, it is possible that they do not show the narrow spectra from the wind due to the non-steady mass loss of their progenitors. When the shock breakout occurs in the dense wind with the density structure $\rho \propto r^{-w}$, the ratio of the diffusion timescale in the optically thick region of the wind (t_d) and the shock propagation timescale of the entire wind (t_s) after the shock breakout strongly depends on w . For the case $w \lesssim 1$, both timescales are comparable ($t_d/t_s \simeq 1$) and t_d/t_s gets smaller as w gets larger. For the case $t_d/t_s \simeq 1$, the shock goes through the entire wind just after the light curve (LC) peak and narrow spectral lines from the wind cannot be observed after the LC peak (Type IIL LSNe). If t_d/t_s is much smaller, the shock wave continues to propagate in the wind after the LC peak and unshocked wind remains (Type IIn LSNe). This difference can only be obtained through a careful treatment of the shock breakout condition in a dense wind. The lack of narrow Lorentzian line profiles in Type IIL LSNe before the LC peak can also be explained by the difference in the density slope. Furthermore, we apply our model to Type IIn LSN 2006gy and Type IIL LSN 2008es and find that our model is consistent with the observations.

Subject headings: supernovae: general — supernovae: individual (SN 2006gy, SN 2008es) — stars: mass-loss — shock waves — radiative transfer

1. INTRODUCTION

Shock breakout is a phenomenon which is predicted to be observed when a shock wave emerges from the surface of an exploding star. Before the shock wave approaches the surface of the star, the diffusion timescale of photons is much longer than the dynamical timescale of the shock wave because of the high optical depth of the stellar interior and photons cannot go out of the shock wave. At the stellar surface, the optical depth above the shock wave suddenly becomes low enough for photons to diffuse out from the shock wave and photons start to travel away from the star. This sudden release of photons is predicted to be observed as a flash of X-rays or ultraviolet (UV) photons (e.g., Ohya 1963; Colgate 1974; Klein & Chevalier 1978; Ensmann & Burrows 1992; Matzner & McKee 1999; Nakar & Sari 2010; Tominaga et al. 2011) and actually observed for several times, e.g., XRO 080109/SN 2008D (e.g., Soderberg et al. 2008) and SNLS-04D2dc (Schawinski et al. 2008; Gezari et al. 2009).

If the circumstellar wind of the SN progenitor is dense and optically thick, the shock breakout signal is altered by the wind. Photons emitted from the shock dif-

fuse in the wind and the light curve (LC) of the shock breakout becomes broader (e.g., Falk & Arnett 1977; Grasberg & Nadezhin 1987; Moriya et al. 2011). If the wind is much denser, the shock breakout itself can take place in the wind. The shock breakout in the dense wind is related to astrophysical phenomena, e.g., PTF 09uj (Ofek et al. 2010), XRO 080109 (Balberg & Loeb 2011), and production of high energy particles (Murase et al. 2011; Katz et al. 2011). In particular, Chevalier & Irwin (2011) associate luminous supernovae (LSNe) to the shock breakout in the dense wind.

Many LSNe are believed to be brightened by the shock interaction between SN ejecta (or materials released from stellar surface) and the dense circumstellar wind (e.g., Smith & McCray 2007; Woosley et al. 2007; van Marle et al. 2010; Blinnikov & Sorokina 2010)⁵. This is because many LSNe are spectroscopically classified as Type IIn, which shows narrow spectral lines from the wind surrounding SN ejecta⁶ (e.g., Smith et al. 2010; Drake et al. 2010; Rest et al. 2011; Chatzopoulos et al. 2011; Drake et al. 2011). For example, SN 2006gy shows Lorentzian H Balmer lines with the full width at half maximum velocity $\simeq 1,000 \text{ km s}^{-1}$ (e.g., Smith et al. 2010) which are suggested to originate from the dense wind (e.g., Chugai 2001; Chugai et al. 2004; Dessart et al. 2009). In addition, SN 2006gy shows nar-

¹ Institute for the Physics and Mathematics of the Universe, Todai Institutes for Advanced Study, University of Tokyo, Kashiwanoha 5-1-5, Kashiwa, Chiba 277-8583, Japan; takashi.moriya@ipmu.jp

² Department of Astronomy, Graduate School of Science, University of Tokyo, Hongo 7-3-1, Bunkyo, Tokyo 113-0033, Japan

³ Research Center for the Early Universe, Graduate School of Science, University of Tokyo, Hongo 7-3-1, Bunkyo, Tokyo 113-0033, Japan

⁴ Department of Physics, Faculty of Science and Engineering, Konan University, Okamoto 8-9-1, Kobe, Hyogo 658-8501, Japan

⁵ There are other suggestions for an energy source to brighten LSNe: e.g., huge amount of ⁵⁶Ni produced during SN explosions (e.g., Gal-Yam et al. 2009; Young et al. 2010; Moriya et al. 2010), newly born magnetars (e.g., Maeda et al. 2007; Kasen & Bildsten 2010; Woosley 2010), and optical afterglows of gamma-ray bursts (e.g., Young et al. 2005).

⁶ See, for example, Schlegel (1990); Filippenko (1997) for the spectral classification of Type IIn and other SN types.

row P-Cygni profile from $\simeq 100 \text{ km s}^{-1}$ outflow which is also presumed to stem from the wind surrounding the SN ejecta (e.g., Smith et al. 2010). However, there commonly exist LSNe without narrow spectral lines from the circumstellar wind (e.g., Quimby et al. 2007; Miller et al. 2009; Gezari et al. 2009; Pastorello et al. 2010; Quimby et al. 2011; Chomiuk et al. 2011). Based on the LC shapes of LSNe, Chevalier & Irwin (2011) show that, if the shock breakout takes place inside the dense wind, the SN is observed as SN 2006gy-like Type IIn LSNe and, if it takes place at the surface, the SN is observed as SN 2010gx-like non-Type IIn LSNe.

In the previous works of the shock breakout in a dense wind, the density slope of the wind has been assumed to be $\simeq -2$ which is a consequence of the steady mass loss of the progenitor. However, non-steady mass loss is actually observed in the massive stars which are suggested to be possible progenitors of LSNe, e.g., η Carinae (e.g., Davidson & Humphreys 1997; Gal-Yam & Leonard 2009). In addition, historical X-ray SN observations are suggested to indicate that mass loss from progenitors of Type IIn SNe is inconsistent with the steady mass loss (Dwarkadas & Gruszko 2011). Here, we investigate the influence of non-steady mass loss on the shock breakout in the dense wind and show that the diversity in the wind density slope caused by the non-steady mass loss can explain why some Type II LSNe show narrow spectral components from the wind while others do not even if both LSNe are illuminated by the shock interaction. Our model is presented in Section 2 and it is applied to LSNe in Section 3. We discuss our results in Section 4. Conclusions are summarized in Section 5.

2. EFFECT OF DENSE NON-STEADY WIND

2.1. Wind Configuration

We consider a spherically symmetric dense wind extending from $r = R_i$ to $r = R_o$ where r is radius. The density ρ is assumed to follow $\rho(r) = Dr^{-w}$ with a constant D . The opacity κ of the wind is assumed to be constant throughout this paper. We assume that a SN explosion has occurred in the dense wind and that the shock breakout occurs in the wind (e.g., Chevalier & Irwin 2011, see Section 1). The radius of the forward shock at the time of the shock breakout is set to $r = xR_o$. Note that the entire wind above the progenitor star is optically thick because of the assumption that the shock breakout occurs in the dense wind. We also introduce a radius $y_\tau R_o$ where the optical depth evaluated from the surface becomes τ , i.e.,

$$\tau = \int_{y_\tau R_o}^{R_o} \kappa \rho dr. \quad (1)$$

2.2. Shock Breakout Condition in Non-Steady Dense Wind

Shock breakout in a wind had been simply defined to occur when the diffusion timescale of the entire wind is comparable to the shock propagation timescale of the entire wind, i.e. (see, e.g., Weaver 1976; Nakar & Sari 2010, for the details of the shock breakout condition),

$$\int_{xR_o}^{R_o} \kappa \rho dr \simeq \frac{c}{v_s}. \quad (2)$$

However, the wind could contain large optically thin region even if the entire wind is optically thick. Figure 1 is a simplified illustration of the effect of w in the dense wind. Two dense winds with the different w but the same R_o and xR_o are compared in the figure: (a) a wind with a constant density and (b) a wind with a steep density gradient. In both cases, the shock breakout is assumed to occur in the wind at the same radius $r = xR_o$ ($x < 1$) with the same forward shock velocity v_s and thus the optical depth between xR_o and R_o is exactly the same in both cases (τ_b). One of the important differences in the two winds are in the radius of the last scattering surface $y_1 R_o$, where $\tau = 1$ (see Figure 2 in the following for the value of y_1). Even if the entire wind is optically thick in both cases, the region where τ becomes larger than 1 ($r < y_1 R_o$) is more concentrated to the central region and the wind contains large optically thin region outside whose size is $\Delta R = R_o - y_1 R_o$ in the case of large w .

If the wind contains an extended optically thin region, Equation (2) is no longer an appropriate condition for the shock breakout because it postulates that the entire wind at $r \leq R_o$ is optically thick enough for photons to be diffusive. The shock breakout condition should be evaluated only at the optically thick region where photons are diffusive. Thus, the shock breakout should occur when the diffusion timescale of the optically thick region of the wind is comparable to the shock propagation timescale of the region. Hence, the shock breakout condition is set to

$$\tau_x \equiv \int_{xR_o}^{y_1 R_o} \kappa \rho dr \simeq \frac{c}{v_s}, \quad (3)$$

where c is the speed of light and $\tau_x = \tau_b - 1$. In Equation (3), we presume that photons diffuse in the region where the optical depth evaluated from the wind surface exceeds 1 for simplicity. I.e., photons are assumed to diffuse at $R_i < r < y_1 R_o$ and freely stream at $y_1 R_o < r < R_o$. In this sense, Equation (3) may also be interpreted as Equation (2) combined with a kind of flux limited diffusion approximation. For the case of the shock breakout at the surface of the wind ($x \simeq 1$), the conditions of Equations (2) and (3) are similar.

Since the observations of Type II LSNe display a constant shock velocity (e.g., Smith et al. 2010), we assume that the SN ejecta is freely expanding and v_s is constant. Equations (1) and (3) lead us to

$$D \simeq \begin{cases} \frac{(1-w)(1+c/v_s)}{\kappa(1-x^{1-w})R_o^{1-w}} & (w \neq 1), \\ \frac{1+c/v_s}{\kappa(-\ln x)} & (w = 1). \end{cases} \quad (4)$$

In addition, using Equation (4), we can express y_τ as

$$y_\tau \simeq \begin{cases} \left(\frac{c/v_s + \tau x^{1-w}}{c/v_s + \tau} \right)^{\frac{1}{1-w}} & (w \neq 1), \\ x^{\frac{\tau}{c/v_s + \tau}} & (w = 1). \end{cases} \quad (5)$$

Figure 2 shows a plot of y_1 as a function of x for several w . The larger w is, the smaller y_1 becomes for a given x , as is discussed qualitatively above.

Finally, the wind mass M_{wind} is defined as

$$M_{\text{wind}} = \int_{R_i}^{R_o} 4\pi r^2 \rho dr. \quad (6)$$

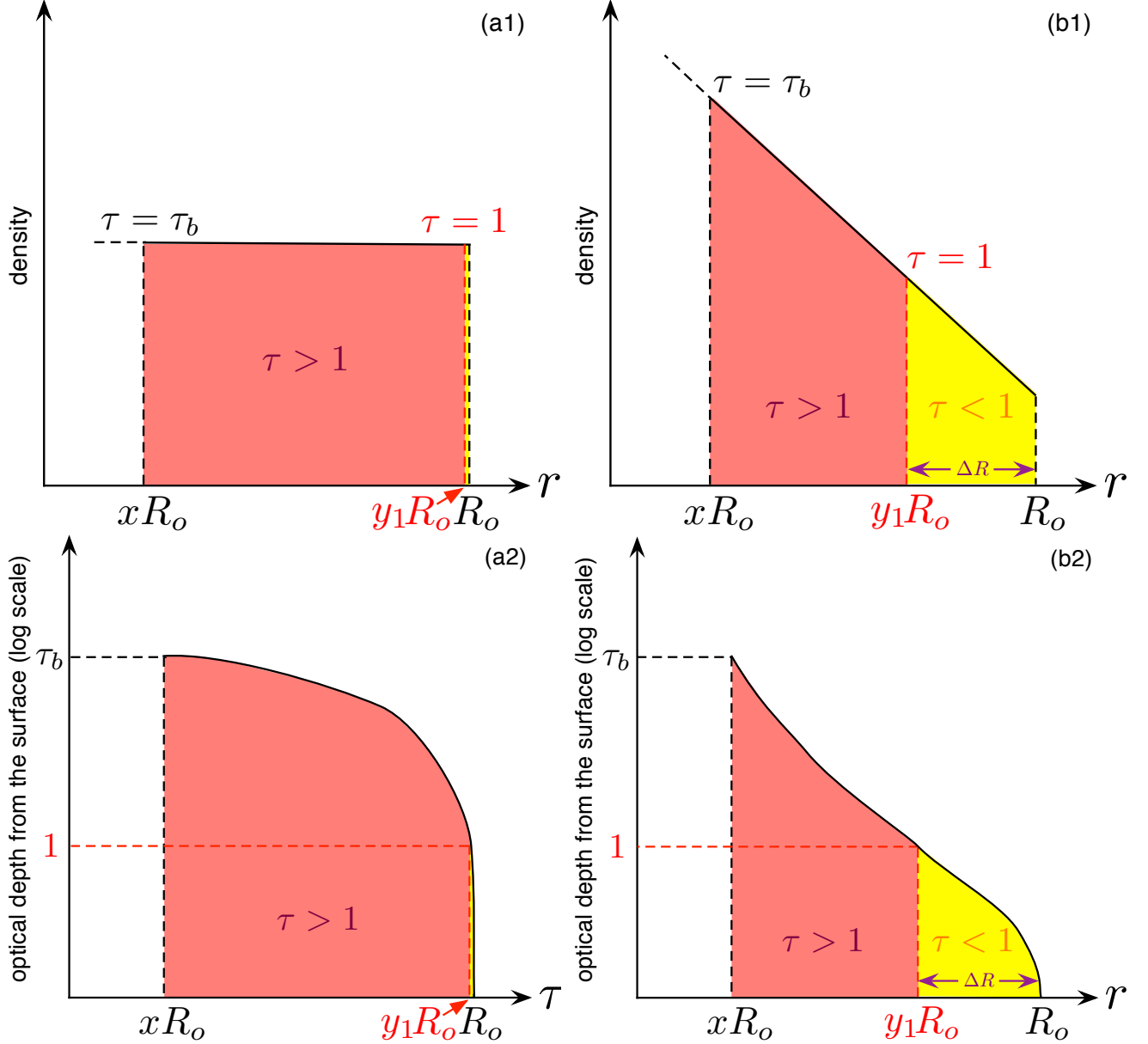


FIG. 1.— Illustration of the density and the optical depth distributions for the winds with different density slopes: (a) a flat density slope and (b) a steep density slope. The corresponding (1) density structures and (2) optical depth distributions are shown. The shock breakout is assumed to occur at the same $r = xR_o$ with $x < 1$ where opacity τ from R_o becomes τ_b . All the opacities shown in the figure is evaluated from R_o . Large $\tau < 1$ region appears in the outer part of the wind in (b). See Figure 4 for the concrete examples for the distribution.

Using Equation (4), we get

$$M_{\text{wind}} \simeq \begin{cases} \frac{4\pi(1-w)(1+c/v_s)(R_o^{3-w}-R_i^{3-w})}{\kappa(3-w)(1-x^{1-w})R_o^{1-w}} & (w \neq 1, 3), \\ \frac{2\pi(1+c/v_s)(R_o^2-R_i^2)}{\kappa(-\ln x)} & (w = 1), \\ \frac{8\pi(1+c/v_s)\ln(R_o/R_i)}{\kappa(x^{-2}-1)R_o^{-2}} & (w = 3). \end{cases} \quad (7)$$

2.3. Timescales of Photon Diffusion and Shock Propagation in Dense Wind

Here, we estimate the timescale of photon diffusion (t_d) which characterizes the LCs of LSNe and the timescale of the shock propagation (t_s) which represents the timescale for the forward shock to go through the entire wind. t_d

corresponds to the timescale for the LC to reach the peak (e.g., Arnett 1980, 1982). t_d can be expressed as

$$t_d \simeq \frac{\tau_x(R_o - xR_o - \Delta R)}{c} \quad (8)$$

$$= \frac{\tau_x(y_1 - x)R_o}{c} \quad (9)$$

$$= \begin{cases} \frac{R_o}{v_s} \left[\left(\frac{c/v_s + x^{1-w}}{c/v_s + 1} \right)^{\frac{1}{1-w}} - x \right] & (w \neq 1), \\ \frac{R_o}{v_s} \left(x^{\frac{1}{1+c/v_s}} - x \right) & (w = 1). \end{cases} \quad (10)$$

t_s is defined as the time required for the forward shock to go through the entire wind including the optically thin

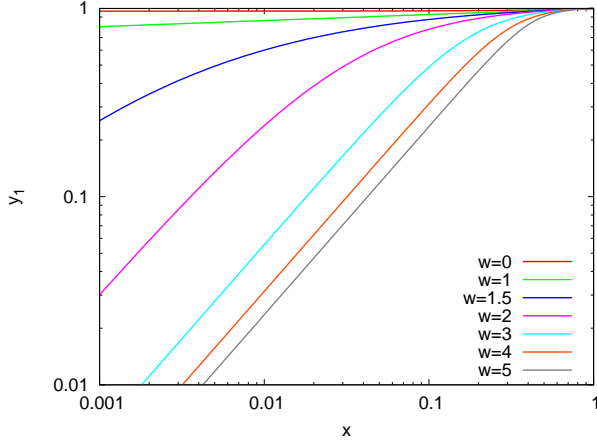


FIG. 2.— Location of the last scattering surface in the wind. The region $r > y_1 R_o$ is optically thin and photons do not diffuse in the region.

region after the shock breakout,

$$t_s = \frac{R_o - xR_o}{v_s}. \quad (11)$$

Hence, we can derive the ratio of the two timescales:

$$\frac{t_d}{t_s} \simeq \begin{cases} \frac{1}{1-x} \left[\left(\frac{c/v_s + x^{1-w}}{c/v_s + 1} \right)^{\frac{1}{1-w}} - x \right] & (w \neq 1), \\ \frac{1}{1-x} \left(x^{\frac{1}{1+c/v_s}} - x \right) & (w = 1). \end{cases} \quad (12)$$

Figure 3 shows the ratio as a function of x with several w , in which v_s is set to $10,000 \text{ km s}^{-1}$, corresponding to the observational value of SN 2008es (see Section 3.2). Every line reaches $t_d/t_s \simeq c/(v_s + c) = 0.97$ at $x \simeq 1$. This corresponds to the case of the shock breakout at the surface of the wind (e.g., Chevalier & Irwin 2011).

When the shock breakout occurs inside the wind ($x < 1$), the ratio t_d/t_s varies depending on the density slope of the wind. For a given x , t_d/t_s gets smaller as the density slope of the wind gets steeper (i.e., larger w). This is because the last scattering surface of the wind locates farther away from the surface as the density slope gets steeper, i.e., y_1 gets smaller as w gets larger for a given x (see Figure 2 for values of y_1). In other words, the optically thin region in the wind is spatially larger for the wind with steeper density gradient. This is true even if the wind radius is the same and also results in small t_d/t_s . We note again that, when the shock breakout occurs in the wind, the forward shock reaches at the last scattering surface ($r = y_1 R_o$) with the diffusion timescale t_d , i.e., the shock locates at $r = y_1 R_o$ at the LC peak.

2.4. Observational Features and Diversities of Interaction-Powered LSNe

In this section, we present consequences from the variation in t_d/t_s which results from the variation in w . We show that the two kinds of Type II LSNe, i.e., Type IIn LSNe (e.g., SN 2006gy, Smith et al. 2010) and Type IIL LSNe (e.g., SN 2008es, Miller et al. 2009; Gezari et al. 2009), are naturally expected from the shock breakout in the dense H-rich wind with the different density slope.

If we assume that both types of LSNe are illuminated by the interaction of the H-rich dense wind and SN ejecta

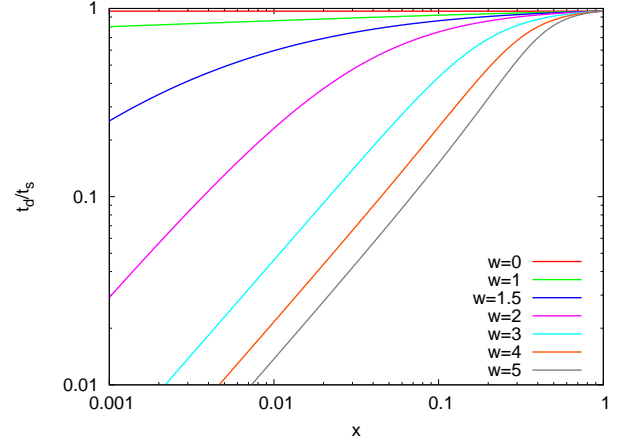


FIG. 3.— Ratio of the diffusion timescale (t_d) and the shock propagation timescale (t_s) as a function of the location of the shock breakout (x).

and that the wind is so dense that the shock breakout occurs in the wind, the spectral evolution of LSNe is determined by t_d/t_s .

If $t_d/t_s \simeq 1$, the shock wave reaches at the surface of the dense wind soon after the LC has reached the peak with the timescale t_d . Since the entire wind is shocked just after the LC peak, no signature in spectra from the wind are observable after the LC peak. On the other hand, if $t_d/t_s < 1$, the shock wave continues to propagate in the optically thin region of the wind even after the LC peak. As there remains unshocked materials in the wind even after the LC peak, we expect to see narrow P-Cygni profiles from the unshocked wind even after the LC peak.

The narrow Lorentzian line profiles which are suggested to be caused by the dense wind (e.g., Chugai 2001; Dessart et al. 2009) can appear before the LC peak depending on the optical depth of the wind. If we apply the model of Chugai (2001), the ratio U of the unscattered H α line flux to the total H α line flux of the Lorentzian profile is

$$U \simeq \frac{1 - e^{-\tau}}{\tau}. \quad (13)$$

For the case of flat density slopes, τ remains too high until the forward shock reaches near the surface (Figure 1) and U is expected to be very small for a long time before the LC peak. On the other hand, if the density decline is steep, the optical depth decreases gradually with time and the suitable optical depth would be realized for a long while. Therefore, Lorentzian lines are expected to be observed well before the LC peak.

To sum up, Type IIL LSNe can come from the dense wind with $t_d/t_s \simeq 1$ while Type IIn LSNe can result from the dense wind with $t_d/t_s < 1$. The ratio of the two timescales is determined by w .

The LC evolution of Type II LSNe are also consistent with our models. In our models for both Type IIn and Type IIL LSNe, the forward shock stays in the dense wind until the LC peak. As the wind with $\tau > 1$ is shocked with the timescale of t_d , the dense wind adiabatically cools down after the LC peak. Thus, the LCs of Type II LSNe are supposed to follow the shell-shocked diffusion model presented by Smith & McCray (2007). The shell-shocked diffusion model is based on the adia-

batic cooling of the shocked dense wind, which is basically the same as the LC model suggested for Type II SNe by Arnett (1980), and the model had been already shown to be consistent with the declining phase of the LC of SN 2006gy (Smith & McCray 2007).

3. COMPARISON WITH OBSERVATIONS

In the previous section, we have shown that, if the shock breakout occurs inside a dense wind ($x < 1$), the ratio between the timescales of the photon diffusion and the shock propagation in the wind depends on the wind density slope and thus the different density slope can result in two kinds of Type II LSNe, i.e., Type IIn and Type IIL LSNe. As an example, we apply our model to two LSNe: Type IIn SN 2006gy and Type IIL SN 2008es. If we look into Type IIn LSN 2006gy and Type IIL LSN 2008es, one important difference is in the existence of narrow P-Cygni profiles in the spectra of SN 2006gy after the LC peak. According to the observational feature, we can guess that Type IIL LSN 2008es came from the dense wind with $t_d/t_s \simeq 1$ while Type IIn LSN 2006gy resulted from the dense wind with $t_d/t_s < 1$. We apply those models to the two LSNe. In this section, κ is set to $0.34 \text{ cm}^2 \text{ g}^{-1}$.

3.1. Type IIn LSNe (SN 2006gy)

SN 2006gy is extensively studied by, e.g., Ofek et al. (2007); Smith et al. (2007); Smith & McCray (2007); Woosley et al. (2007); Smith et al. (2008); Agnoletto et al. (2009); Kawabata et al. (2009); Smith et al. (2010); Miller et al. (2010). It is classified as Type IIn and the luminosity reaches ~ -22 mag in the R band (Smith et al. 2007). The detailed spectral evolution are summarized in Smith et al. (2010). The narrow P-Cygni $\text{H}\alpha$ with the absorption minimum of $\simeq 100 \text{ km s}^{-1}$ is considered to come from the wind surrounding the progenitor of SN 2006gy. As SN 2006gy show narrow P-Cygni profiles after the maximum luminosity, unshocked wind is supposed to remain after the maximum. Thus, models with $t_d/t_s < 1$ and $y_1 < 1$ are preferred. Based on the observations of Smith et al. (2010), we adopt the following parameters:

$$v_s \simeq 5,200 \text{ km s}^{-1}, \quad (14)$$

$$t_d \simeq 70 \text{ days}. \quad (15)$$

v_s is constrained by the evolution of the blackbody radius and t_d is obtained from the rising time of the LC. As the narrow $\text{H}\alpha$ P-Cygni profile is detected at 179 days⁷ and disappears at 209 days (Smith et al. 2010), we presume that the forward shock has gone through the entire wind between 179 days and 209 days. We simply take the central date (194 days) as the time when the forward shock has gone through the entire wind, i.e., $t_s \simeq 194$ days. With t_d , t_s , and v_s , we can estimate x and R_o for a given w from Equations (10) and (11).

If we adopt the model with $w = 2$, for example, x and R_o are estimated to be 0.0095 and $8.8 \times 10^{15} \text{ cm}$, respectively. In this case, shock breakout occurs at $xR_o \simeq 3.2 \times 10^{14} \text{ cm}$ and the last scattering surface is $y_1R_o \simeq 3.2 \times 10^{15} \text{ cm}$. The total wind mass is

⁷ Days since the explosion. The explosion date is set to be the same as in Smith et al. (2010).

$M_{\text{wind}} \simeq 0.81 M_{\odot}$ (c.f. $R_i \ll R_o$) and is much smaller than the value estimated from the shell-shocked diffusion LC model ($\sim 10 M_{\odot}$; Smith et al. 2010). Alternatively, if we adopt steeper density gradient with $w = 5$, x and R_o are estimated to be 0.17 and $1.05 \times 10^{16} \text{ cm}$, respectively, and thus $xR_o \simeq 1.8 \times 10^{15} \text{ cm}$ and $y_1R_o \simeq 4.9 \times 10^{15} \text{ cm}$. y_1R_o is consistent with the blackbody radius at the LC peak estimated from the observations ($6 \times 10^{15} \text{ cm}$). If we assume that $R_i \simeq 10^{15} \text{ cm}$, the mass contained in the optically thick region ($R_i < r < y_1R_o$) is $22 M_{\odot}$ in our $w = 5$ model, which is comparable to the mass obtained by Smith & McCray (2007). In this case, the mass of the entire wind becomes $M_{\text{wind}} \simeq 23 M_{\odot}$. The left panel of Figure 4 is the optical depth and the enclosed mass distributions. The existence of the unshocked wind may also account for the weakness of the X-ray emission of SN 2006gy (e.g., Woosley et al. 2007).

The spectral evolution of SN 2006gy is also consistent with our model. Lorentzian H Balmer lines seen in the spectra of SN 2006gy are presumed to be caused by the optically thick wind (e.g., Chugai 2001; Dessart et al. 2009). For example, for the case $w = 5$, τ become $\simeq 10$ at around $3 \times 10^{15} \text{ cm}$ (Figure 4). This is consistent with $\tau \simeq 15$ at 36 days which is estimated from the observed ratio U derived from $\text{H}\alpha$ (Smith et al. 2010). In our model, the Lorentzian line profiles are expected to be observed before the forward shock wave goes through the optically thick region of the wind, i.e., before t_d , and thus, the Lorentzian spectra should disappear after the LC peak. This is also consistent with the spectra of SN 2006gy (Smith et al. 2010).

Narrow $\text{H}\alpha$ P-Cygni profiles can be created at the optically thin wind above the last scattering surface of the continuum photons ($y_1R_o < r < R_o$) because of the larger line opacities. Whether the narrow $\text{H}\alpha$ P-Cygni profiles can form or not depends also on the ionization level of the wind and thus the spectral modeling must be performed to see whether the narrow $\text{H}\alpha$ profiles are actually synthesized in the unshocked wind in our model.

3.2. Type IIL LSNe (SN 2008es)

Here, we apply our model to SN 2008es which is one of the best observed Type IIL LSNe (Miller et al. 2009; Gezari et al. 2009). Although SN 2008es does not show any features of the wind in the spectra, we assume that it is also illuminated by the interaction based on their brightness, rapid decline of the LC, and blue spectra. In our model, the lack of the wind features after the LC peak can be explained by the small difference in t_d and t_s because the entire wind is shocked by the forward shock just after the LC peak. In other words, y_1 should be close to 1. This can be achieved by the wind slope with $w \lesssim 1$ for the case of $x < 1$ (Figure 2).

The following parameters are estimated from the observations:

$$v_s \simeq 10,000 \text{ km s}^{-1}, \quad (16)$$

$$t_d \simeq t_s \simeq 23 \text{ days}. \quad (17)$$

If we adopt the model of $w = 0$, y_1 is close to 1 and $R_o \simeq v_s t_s \simeq y_1 R_o \simeq 2 \times 10^{15} \text{ cm}$. $y_1 R_o$ is consistent with the blackbody radius at the LC peak estimated from the observations ($3 \times 10^{15} \text{ cm}$). Assuming $x = 0.1$ and $R_i \ll R_o$, the wind mass is $M_{\text{wind}} \simeq 0.85 M_{\odot}$. M_{wind} does not vary so much on x unless it is close

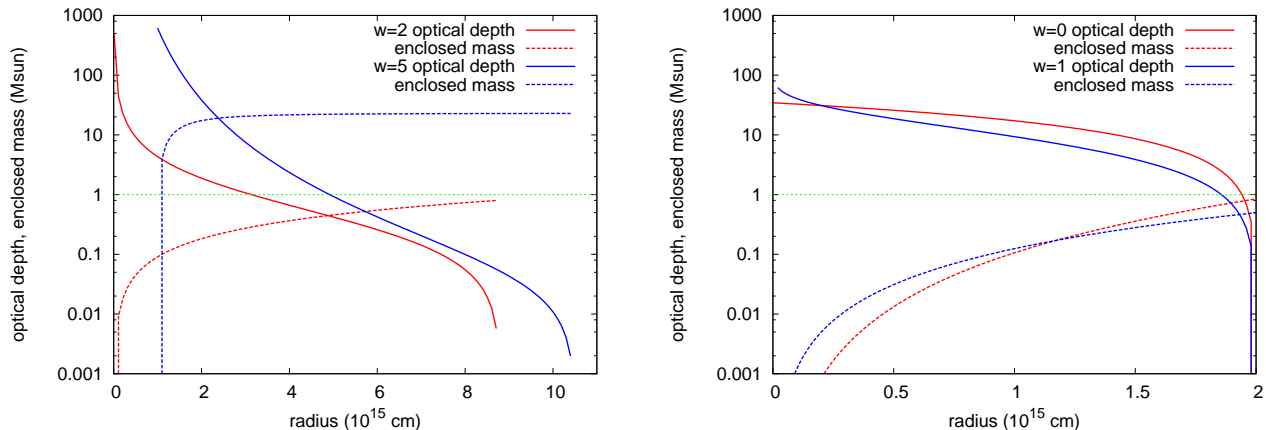


FIG. 4.— *Left*: Optical depth and enclosed mass distribution of the models $w = 2$ and $w = 5$ applied for LSN 2006gy. *Right*: Same as the left panel but for the models of LSN 2008es ($w = 0, 1$).

to 1. The model with $w = 1$ also gives $y_1 \simeq 1$ with $M_{\text{wind}} \simeq 0.50 M_{\odot}$. The right panel of Figure 4 shows the optical depth and mass distributions. Miller et al. (2009) estimate $M_{\text{wind}} \simeq 5 M_{\odot}$ based on the shell-shocked diffusion LC model of Smith & McCray (2007). Gezari et al. (2009) obtained $M_{\text{wind}} \simeq 0.2 M_{\odot}$ based on the peak luminosity. M_{wind} of both $w = 0$ and $w = 1$ models are almost consistent with those estimates.

Lack of the Lorentzian H Balmer lines before the LC peak is another important difference between Type IIL LSN 2008es and Type IIn LSN 2006gy. For the case of the flat density slope, the wind optical depth remains to be very large until the forward shock reaches near the wind surface (Figure 4). Hence, narrow H lines, even if they are emitted from the dense region of the wind, are scattered by the dense wind with a large optical depth for a long while. Then, U will be very small until the forward shock reaches near the wind surface and the Lorentzian H lines will be very weak. Thus, it is likely that the Lorentzian H lines emitted from the dense wind are missed. Detailed modeling is required to see the actual spectral evolution expected from the density profile of our model.

4. DISCUSSION

We have shown that the difference in density slopes of dense winds can make a variety of LSNe after the shock breakout in the dense wind. Flat density slopes result in Type IIL LSNe and steep density slopes result in Type IIn LSNe. The model with the shock breakout in the dense wind is recently applied to LSNe by Chevalier & Irwin (2011). Their idea for SN 2006gy is basically the same as our suggestion for Type IIn LSNe: the shock breakout inside the dense wind ($x < 1$). However, as they only consider the case $w = 2$, non-Type IIn LSNe are related to the shock breakout at the surface ($x \simeq 1$) of the dense wind. In this paper, we show that the shock breakout does not necessarily occur at the surface to explain non-Type IIn LSNe, especially Type IIL LSNe when the progenitor star experiences the non-steady mass loss. Currently, both models can explain Type IIL LSNe. For the case of the shock breakout inside the dense wind ($x < 1$), the Lorentzian spectral lines might be able to be observed just before the LC peak when the suitable optical depth is realized. The

detailed spectral observations near the LC peak can distinguish the two scenario. Note that we do not exclude the possibility that steep density slopes can become Type IIL LSNe. If the density is high enough up to the surface, steep dense winds can end up with Type IIL LSNe, i.e., y_1 become close 1 at $x = 1$ no matter what the density decline is. This configuration corresponds to the shock breakout at the surface and exactly the same as what is suggested by Chevalier & Irwin (2011).

An important difference between our treatment of the shock breakout in a dense wind from that of the previous works is that we are not using Equation (2) for the shock breakout condition but Equation (3). If we use Equation (2), the differences caused by the different density slopes are missed. For example, with Equation (2), we do not expect see narrow spectral lines from the dense wind after the LC peak of all LSNe with shock breakout in the dense wind and they are all expected to be observed as Type IIL SNe. This is because the forward shock is regarded to go through the entire wind at the LC peak in Equation (2).

The different density slope in the dense wind is naturally expected to be caused by the non-steady mass loss of the progenitor just before the explosion⁸. If Type IIL LSNe are actually caused by the shock breakout in the wind with $t_d/t_s \simeq 1$, it indicates that non-steady mass loss producing the flat dense wind ($w \lesssim 1$) may take place just before the explosions of some massive stars. In addition, our model for Type IIn LSN 2006gy prefers $w \neq 2$ because M_{wind} of the $w = 2$ model is too small to account for the LC of SN 2006gy after the peak. This also supports the existence of the non-steady mass loss at the pre-SN stage of the massive stars. Dwarkadas & Gruszko (2011) show that the density slope of the wind estimated from X-ray observations of Type IIn SNe is inconsistent with $\rho \propto r^{-2}$. They show that Type IIn SNe do not usually come from the steady wind with $\rho \propto r^{-2}$. X-ray luminous Type IIn SNe are presumed to be originated

⁸ Note that the flat density distribution of the wind can also be caused by the steady mass loss of two different evolutionary stages (e.g., Dwarkadas 2011). Although the model shown in Dwarkadas (2011) is not dense enough to result in LSNe, the flat density slope might result in Type IIL LSNe if sufficiently high density is achieved.

from relatively dense winds with high mass-loss rates. Although the wind densities of these SNe are not high enough to be LSNe, it is highly possible that the dense winds from higher mass-loss rates also result in flat or steep density slopes. The presence of the two kinds of slopes can end up with two different kinds of Type II LSNe.

So far, we just consider a single slope for the dense wind. One essential difference between Type IIn and Type IIL LSNe is the existence of the spatially-large optically-thin region in the wind of Type IIn LSNe which can make narrow P-Cygni profiles. Although we show that the large w can make such spatially-large optically-thin region with the optically thick region inside, the similar condition can also be achieved by assuming the two components in the wind, i.e., optically thin and thick regions with any density slopes. The two-component wind configuration is suggested for, e.g., Type IIn SN 1998S (Chugai 2001). Both models can explain the Type IIn LSNe. In either case, the P-Cygni profiles can be observed not only after but also before the LC peak. Currently, there are no spectral observations of Type IIn LSNe before the LC peak with the resolution sufficient to resolve the narrow P-Cygni profile and the high resolution spectroscopic observations before the LC peak are important to reveal the wind surround LSNe.

Our model cannot be simply adopted to the spectral evolution of other kinds of LSNe without H lines. Especially, Type Ic LSNe with fast LC decline (e.g., Quimby et al. 2011; Pastorello et al. 2010; Chomiuk et al. 2011) show, e.g., Si and O lines which are not seen in Types II LSNe. Although it is possible that the shock breakout in the dense wind also occurs in Type Ic LSNe as is suggested by Chevalier & Irwin (2011), it seems to be difficult to simply attribute the difference between Type Ic LSNe and Type II LSNe only to the density slope of the dense wind. For example, the composition of the wind is presumed to be quite different between Type Ic and Type II LSNe. If the shock breakout in the dense wind is also taking place in Type Ic LSNe, narrow spectral lines from the materials other than H may be observed.

5. CONCLUSIONS

We investigate the effect of the non-steady mass loss on the shock breakout in the dense wind. The non-steady

mass loss varies the density slope of the wind ($\rho \propto r^{-w}$) and the density slope alters the ratio of the diffusion timescale in the optically thick wind (t_d) and the shock propagation timescale of the entire wind (t_s) after the shock breakout in the wind. Both timescales are comparable ($t_d/t_s \simeq 1$) for $w \lesssim 1$ and t_d/t_s becomes smaller as w gets larger. This is because the last scattering surface of the dense wind locates farther inside from the wind surface for the wind with the steeper density gradient (Figure 2). This difference can only be obtained by the careful treatment of the shock breakout condition in a dense wind (Section 2; Equation (3)).

If the two timescales are comparable ($t_d/t_s \simeq 1$ or $w \lesssim 1$), the forward shock goes through the entire wind just after the LC reaches the peak with the timescale t_d . In this case, no signature on spectra from the wind are expected to be observed especially after the LC peak because the entire wind is already shocked after the LC peak. On the other hand, if the two timescales are different ($t_d/t_s < 1$ or large w), the shock continues to propagate in the wind after the LC peak and the unshocked wind remains after the LC peak. Thus, narrow P-Cygni profiles from the wind are expected to be observed even after the LC peak. The former case corresponds to Type IIL LSNe and the latter to Type IIn LSNe. The difference in the density slope can also account for the lack of the Lorentzian emission profiles in Type IIL LSNe.

Our results imply that the luminosity of Type IIL LSNe can be explained in the context of the shock interaction between SN ejecta and the dense wind even if they do not show the signature of the wind in their spectra. We propose that the difference between Type IIn and Type IIL LSNe can stem from the density slope of the dense wind which results from the non-steady mass loss of their progenitors.

We thank Sergei I. Blinnikov for continuous discussion regarding to radiation hydrodynamics. We also thank Keiichi Maeda for discussion. T.M. is supported by the Japan Society for the Promotion of Science Research Fellowship for Young Scientists. This research is also supported by World Premier International Research Center Initiative, MEXT, Japan.

REFERENCES

- Agnoletto, I., Benetti, S., Cappellaro, E., et al. 2009, *ApJ*, 691, 1348
 Arnett, W. D. 1982, *ApJ*, 253, 785
 Arnett, W. D. 1980, *ApJ*, 237, 541
 Balberg, S., & Loeb, A. 2011, *MNRAS*, 414, 1715
 Blinnikov, S. I., & Sorokina, E. I. 2010, arXiv:1009.4353
 Chatzopoulos, E., Wheeler, J. C., Vinko, J., et al. 2011, *ApJ*, 729, 143
 Chevalier, R. A., & Irwin, C. M. 2011, *ApJ*, 729, L6
 Chomiuk, L., Chornock, R., Soderberg, A. M., et al. 2011, arXiv:1107.3552
 Chugai, N. N. 2001, *MNRAS*, 326, 1448
 Chugai, N. N., Blinnikov, S. I., Cumming, R. J., et al. 2004, *MNRAS*, 352, 1213
 Colgate, S. A. 1974, *ApJ*, 187, 333
 Davidson, K., & Humphreys, R. M. 1997, *ARA&A*, 35, 1
 Dessart, L., Hillier, D. J., Gezari, S., Basa, S., & Matheson, T. 2009, *MNRAS*, 394, 21
 Drake, A. J., Djorgovski, S. G., Mahabal, A., et al. 2011, *ApJ*, 735, 106
 Drake, A. J., Djorgovski, S. G., Prieto, J. L., et al. 2010, *ApJ*, 718, L127
 Dwarkadas, V. V. 2011, *MNRAS*, 412, 1639
 Dwarkadas, V. V., & Gruszko, J. 2011, arXiv:1109.2616
 Ensmann, L., & Burrows, A. 1992, *ApJ*, 393, 742
 Falk, S. W., & Arnett, W. D. 1977, *ApJS*, 33, 515
 Filippenko, A. V. 1997, *ARA&A*, 35, 309
 Gal-Yam, A., & Leonard, D. C. 2009, *Nature*, 458, 865
 Gal-Yam, A., Mazzali, P., Ofek, E. O., et al. 2009, *Nature*, 462, 624
 Gezari, S., Halpern, J. P., Grupe, D., et al. 2009, *ApJ*, 690, 1313
 Gezari, S., Dessart, L., Basa, S., et al. 2008, *ApJ*, 683, L131
 Grasberg, E. K., & Nadezhin, D. K. 1987, *Soviet Ast.*, 31, 629
 Kasen, D., & Bildsten, L. 2010, *ApJ*, 717, 245
 Katz, B., Sapir, N., & Waxman, E. 2011, arXiv:1106.1898
 Kawabata, K. S., Tanaka, M., Maeda, K., et al. 2009, *ApJ*, 697, 747

- Klein, R. I., & Chevalier, R. A. 1978, *ApJ*, 223, L109
- Maeda, K., Tanaka, M., Nomoto, K., et al. 2007, *ApJ*, 666, 1069
- Matzner, C. D., & McKee, C. F. 1999, *ApJ*, 510, 379
- Miller, A. A., Chornock, R., Perley, D. A., et al. 2009, *ApJ*, 690, 1303
- Miller, A. A., Smith, N., Li, W., et al. 2010, *AJ*, 139, 2218
- Moriya, T., Tominaga, N., Blinnikov, S. I., Baklanov, P. V., & Sorokina, E. I. 2011, *MNRAS*, 415, 199
- Moriya, T., Tominaga, N., Tanaka, M., Maeda, K., & Nomoto, K. 2010, *ApJ*, 717, L83
- Murase, K., Thompson, T. A., Lacki, B. C., & Beacom, J. F. 2011, *Phys. Rev. D*, 84, 043003
- Nakar, E., & Sari, R. 2010, *ApJ*, 725, 904
- Ofek, E. O., Cameron, P. B., Kasliwal, M. M., et al. 2007, *ApJ*, 659, L13
- Ofek, E. O., Rabinak, I., Neill, J. D., et al. 2010, *ApJ*, 724, 1396
- Ohyama, N. 1963, *Progress of Theoretical Physics*, 30, 170
- Pastorello, A., Smartt, S. J., Botticella, M. T., et al. 2010, *ApJ*, 724, L16
- Quimby, R. M., Kulkarni, S. R., Kasliwal, M. M., et al. 2011, *Nature*, 474, 487
- Quimby, R. M., Aldering, G., Wheeler, J. C., et al. 2007, *ApJ*, 668, L99
- Rest, A., Foley, R. J., Gezari, S., et al. 2011, *ApJ*, 729, 88
- Schawinski, K., Justham, S., Wolf, C., et al. 2008, *Science*, 321, 223
- Schlegel, E. M. 1990, *MNRAS*, 244, 269
- Smith, N., Chornock, R., Silverman, J. M., Filippenko, A. V., & Foley, R. J. 2010, *ApJ*, 709, 856
- Smith, N., Foley, R. J., Bloom, J. S., et al. 2008, *ApJ*, 686, 485
- Smith, N., Li, W., Foley, R. J., et al. 2007, *ApJ*, 666, 1116
- Smith, N., & McCray, R. 2007, *ApJ*, 671, L17
- Soderberg, A. M., Berger, E., Page, K. L., et al. 2008, *Nature*, 453, 469
- Tominaga, N., Morokuma, T., Blinnikov, S. I., et al. 2011, *ApJS*, 193, 20
- van Marle, A. J., Smith, N., Owocki, S. P., & van Veelen, B. 2010, *MNRAS*, 407, 2305
- Weaver, T. A. 1976, *ApJS*, 32, 233
- Woosley, S. E. 2010, *ApJ*, 719, L204
- Woosley, S. E., Blinnikov, S., & Heger, A. 2007, *Nature*, 450, 390
- Young, D. R., Smartt, S. J., Valenti, S., et al. 2010, *A&A*, 512, A70
- Young, T. R., Smith, D., & Johnson, T. A. 2005, *ApJ*, 625, L87